Scientific Research Publishing

Journal of Modern Physics, 2025, 16(6), 858-885
https://www.scirp.org/journal/jmp
ISSN Online: 2153-120X
ISSN Print: 2153-1196

Quantum Gravitodynamics Simulation of Hadrons

Edwin Eugene Klingman

Cybernetic Micro Systems, Inc., San Gregorio, CA, USA
Email: klingman@geneman.com

How to cite this paper: Klingman, E.E. (2025) Quantum Gravitodynamics Simulation of Hadrons. *Journal of Modern Physics*, **16**, 858-885.
https://doi.org/10.4236/jmp.2025.166045

Received: May 9, 2025
Accepted: June 22, 2025
Published: June 25, 2025

Abstract

Quantum Chromodynamic hadron models are lattice-QCD simulations with flux tubes terminating on quarks; *Quantum Gravitodynamics* hadron models use flux tube-based parton distributions. QCD is based on color-charge electric analogy; QGD uses mass-based gravitomagnetic analogy. This paper describes the physics and math underlying the model, attempts to determine if the model is stable, presents preliminary simulation results, and discusses limitations and planned extensions.

Keywords

Flux Tube, Gluon, Baryon, Gravitodynamics, Primordial Field, Quark Dynamics, Strong Force, Proton, Neutron, Meson, Quantum Gravity

1. Introduction

Quantum chromodynamics (QCD) straightforwardly extends quantum electrodynamics (QED) based on the fundamental concept of *one* quantum field per particle species. In contrast, quantum gravitodynamics theory (QGD) is based on the singular field to which all fields (weak, strong, electromagnetic, and gravity) are assumed to converge at sufficiently high energy. The goal of both approaches is to usefully explain particle physics, where *useful* is defined as at least predictive, and, ideally, intuitive. QCD predicts flux tube-based physics but is not intuitive. QGD *is* intuitive, with flux tube-based prediction of quantitative dynamics describing qualitative behaviors. Both approaches use Yang-Mills-based flux tubes, albeit defined differently in each. A QCD paper [1] states as established fact that quarks are confined in hadrons, and as fact that the chromoelectric field *between two static quarks* is distributed in flux tubes. While confinement derives from vast quantities of real world experimental data; lattice QCD simulations occur in 2D, 3D, and 4D versions, some assume infinite numbers of colors and chromomag-

netic monopoles. This paper treats as *fact* that quarks are confined in hadrons, and as *strong likelihood* that flux tube behavior is associated with this. Specific flux tube details are based on QGD, focused on 3-quark dynamic hadrons; QCD predominantly focuses on 2-quark static mesons.

QGD laws are functions of density; there is no point mass or energy, no *point particles*, although such can provide convenient calculations, and are used to approximate nucleon structure. Nucleon form factor dynamics in primordial field theory [2] is initially based on composite quarks orbiting a self-induced C-field flux tube with alternating electrical charges interacting with neighbors along the axis of the flux tube, as seen in **Figure 1**. QGD C-fields roughly correspond to QCD gluon fields, while the QGD linear flux tube differs from the Y and Δ form factors of QCD. Primary goals of simulations are to show stability and to determine string tension and flux tube width.

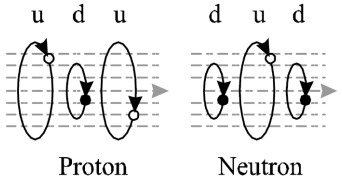

Figure 1. Schematic depiction of proton and neutron form factors.

If e is the charge of the electron, up quarks have electric charge $\frac{2e}{3}$ and down quarks have $\frac{-e}{3}$. In the primordial model of the fermion, a C-field vortex can form a torus, establishing a stability zone that shrinks the torus, potentially without end, and spins increasingly fast, as if the torus converges to a point particle. The appearance of charge, explained by the duality of $\{\boldsymbol{E},\boldsymbol{B}\}$ and $\{\boldsymbol{G},\boldsymbol{C}\}$, will stop the shrinkage; the stronger the charge of the torus, the more quickly the shrinkage is terminated. This implies that the electron is the largest particle, the up quark is next, with the down quark the smallest. In analogy of the skater pulling in her arms to spin faster, the down quark will spin faster than the up quark, which will spin faster than the electron. If $mvr = \frac{\hbar}{2}$, then, as established by our Calabi-Yau derivation of spin-1/2, [3] the momentum, $mv = \frac{h}{4\pi r}$ in agreement with de Broglie's $P = \frac{h}{\lambda}$, the fundamental quantum relation. Material particles will not spin at the speed of light, but if we assume $v \approx c$, then $m \cong \frac{\hbar}{2rc}$. Since spin equates to mass [4], the fastest spinning particle is the most massive, the most point like, and hence the densest.

2. Background of the Theory

Primordial field theory assumes that only *one* field (and *no particles*) existed at

the moment of Creation, while the Standard Model of Particle Physics (SM) assumes that all forces (gravity, electromagnetism, weak, strong) merge into *one* force at the Creation, although unable to demonstrate this theoretically. But if today's forces are considered to merge to one in the beginning, then the converse must hold that the force field present at the beginning, the *primordial field*, should evolve into the particles constituting today's physical reality. A singular field, without particles, will have energy. Since quantum field theory is based on the concept of multiple fields, one per particle type, each particle type being instantiated as an excitation of the corresponding field, quantum field theory (QFT) simply is not applicable to the primordial universe. Quantum theory does not predict anything happening, only the probability of something happening; and is statistical in nature, best understood as an accounting scheme for particle physics. When energies exceed twice the particle energy, new particle-antiparticle pairs can come into existence and the number of particles is undetermined. In QFT pair-creation is expected to occur anywhere at any time, and such *virtual particles* are assumed occasioned by *fluctuations* in the zero-point-energy of the vacuum. Primordial field theory (PFT), like Einstein, assumes vacuum does not exist as pure space and time; space and time are essential qualities of the fundamental field, assumed to be gravity in general relativity. The fundamental formal approach to physics is to assume that change occurs due to physical interactions; with scattering events, leading to S-matrix theory. In PFT there is nothing to interact with other than the field ψ itself, hence fundamental change in ψ, denoted by $\nabla\psi$ consists of the interaction of ψ with itself, written $\psi\psi$. Thus, the fundamental dynamic relation of the primordial field is:

$$\nabla\psi = \psi\psi \tag{1}$$

formulated in terms of a change operator $\nabla \sim \frac{\partial}{\partial\xi}$ with ξ a parametric aspect of the physical entity, denoted by $\psi = \psi(\xi)$, and change in ψ is written $\nabla\psi$. For parametric aspect ξ this equation has a scalar solution $\psi(\xi) = -\xi^{-1}$. If ξ is a vector, we let $\psi\psi = \psi\cdot\psi$ and derive $\psi(\boldsymbol{\xi}) = \boldsymbol{\xi}^{-1}$. Physically, we interpret the scalar parameter as time t and vector parameter as position $\boldsymbol{r}$. If we apply normal field relations, the term $\psi\psi = \psi^2$ is interpreted as field energy density ρ yielding $\nabla\psi = \rho$. If field ψ is gravity $\boldsymbol{G}$, which has negative energy density, then $\boldsymbol{\nabla}\cdot\boldsymbol{G} = \boldsymbol{G}\cdot\boldsymbol{G}$ and

$$\boldsymbol{\nabla}\cdot\boldsymbol{G} = -\rho \tag{2}$$

reduces to Newton's equation, which recovers one of the forces from the primordial field. But Equation (1) was not expressed as inner product $u\cdot v$; the self-interaction equation is $\nabla\psi = \psi\psi$, where ∇ is the difference operator acting on the field ψ, assumed equivalent to the local field interacting with itself. Hestenes [5] defines geometric product $ab = a\cdot b + a\wedge b$ and duality operation $a\wedge b = -i(a\times b)$. Following electromagnetics $(\boldsymbol{E} + i\boldsymbol{B})$ we assume $\psi = \boldsymbol{G} + i\boldsymbol{C}$ and since the solutions are additive, $\nabla = \boldsymbol{\nabla} + \partial_t$, so the expansion contains terms

$\boldsymbol{G}\cdot\boldsymbol{G}$, $\boldsymbol{C}\cdot\boldsymbol{C}$, $\boldsymbol{G}\cdot\boldsymbol{C}$, and derivative terms based on ∇ and ∂_t and Equation (1) becomes

$$(\nabla+\partial_t)(\boldsymbol{G}+i\boldsymbol{C})=(\boldsymbol{G}+i\boldsymbol{C})(\boldsymbol{G}+i\boldsymbol{C}) \tag{3}$$

In calculus derivative operator ∇ is viewed as a vector, so the geometric product of ∇ with a field $\boldsymbol{f}$ is as follows: $\nabla\boldsymbol{f}=\nabla\cdot\boldsymbol{f}+\nabla\wedge\boldsymbol{f}$. This expression, unique to geometric calculus, defines: *gradient* = *divergence* + *curl*. When equation (3) is multiplied out *term by term* all geometric products are expanded and *like terms are grouped* (scalars, *i**scalars, vectors, *i**vectors) to yield:

Self-Interaction equations	**Heaviside equations**	
$\nabla\cdot\boldsymbol{G}=\boldsymbol{G}\cdot\boldsymbol{G}-\boldsymbol{C}\cdot\boldsymbol{C}$	$\nabla\cdot\boldsymbol{G}=-\rho$	(4a)
$i\nabla\cdot\boldsymbol{C}=i2\boldsymbol{G}\cdot\boldsymbol{C}$	$\nabla\cdot\boldsymbol{C}=0$	(4b)
$\partial_t\boldsymbol{G}-\nabla\times\boldsymbol{C}=\boldsymbol{G}\times\boldsymbol{C}\pm\boldsymbol{C}\times\boldsymbol{G}$	$\nabla\times\boldsymbol{C}=-\rho\boldsymbol{v}+\partial_t\boldsymbol{G}$	(4c)
$i\nabla\times\boldsymbol{G}+i\partial_t\boldsymbol{C}=0$	$\nabla\times\boldsymbol{G}=-\partial_t\boldsymbol{C}$	(4d)

$\boldsymbol{G}$ and $\boldsymbol{C}$ are orthogonal fields, so $\boldsymbol{G}\cdot\boldsymbol{C}=\boldsymbol{C}\cdot\boldsymbol{G}\equiv 0$, and $\boldsymbol{G}\cdot\boldsymbol{G}$ and $\boldsymbol{C}\cdot\boldsymbol{C}$ are proportional to energy density of the $\boldsymbol{G}$ and $\boldsymbol{C}$ fields, with $\boldsymbol{G}\times\boldsymbol{C}$ resembling a Poynting vector interpreted as momentum density vector. Grouping like terms and re-expressing the equations in terms of mass density $\rho=\boldsymbol{G}\cdot\boldsymbol{G}+\boldsymbol{C}\cdot\boldsymbol{C}$ and $\rho\boldsymbol{v}\sim\boldsymbol{G}\times\boldsymbol{C}$ the self-interaction equation leads to Heaviside's equations [6] for gravitomagnetism. The field equation of most significance is Heaviside's equation (4c), which, ignoring local change in gravity (*i.e.*, $\frac{\partial G}{\partial t}=0$) is

$$\nabla\times\boldsymbol{C}=-\rho\boldsymbol{v} \tag{5}$$

and which, like Newton's equation for $\boldsymbol{G}$, is density-based. Key to under-standing the current under-appreciation of Heaviside is the realization that in 1916 *Einstein* treated gravity ***as if*** it were geometry, and in this context Heaviside's equation can be derived through linearizing his equation, leading to the mistaken belief that Heaviside was only the "*weak field approximation*" to general relativity, instead of being *completely formally equivalent to GR*. In fact, Einstein's equations are physically meaningless until they make contact with Newton's law of gravity, whereas Newton's law of gravity actually falls out of the Heaviside equation derived from primordial field theory. The unexplained effectiveness of Heaviside's equations in stronger fields, such as those near Black Holes, has been noted [7]. Einstein's equations have been treated in [8] where it is shown how energy density is encoded in geometry, leading to the Schwarzschild metric, and explaining the century-old paradox of *Quasi-Local Mass*, treated in another paper. In the popular view, nevertheless, gravitomagnetic effects are very small and difficult to detect; the effect having been measured by satellites like *Gravity Probe B.* Yet, gravitomagnetic circulation induced by mass current density has an associated energy density. If the matter inducing gravitomagnetic circulation is accelerated, mass current density $\boldsymbol{J}$ changes, which modifies the gravitomagnetic field $\boldsymbol{C}$ and,

in turn, alters the energy density μ_C and equivalent mass density ρ_C, creating a non-linear feedback loop:

$$\boldsymbol{J} \to \boldsymbol{C} \to \mu_C \to \rho_C \to \boldsymbol{J} \tag{6}$$

This non-linearity is based on the self-interaction of the gravitational field and is a key feature of General Relativity that distinguishes it from linear theories like Newtonian gravity, which should, *post-Heaviside* and *post-* $E = mc^2$, be recognized as self-interacting and non-linear. The non-linear feedback loop arising from gravitomagnetic energy density thus implies that the weak field stipulation is insufficient to fully describe the gravitomagnetic effects and the suggestion that gravito-magnetism is only valid in the weak field is not true; gravitomagnetic effects are inherently non-linear and are fully consistent with the non-linear structure of GR. In reality, the gravitomagnetic formalism is applicable at all field strengths and is effectively equivalent to GR.

3. QGD Laws and Equations Are Density-Based

The misleading and incorrect "weak field approximation" has obscured many aspects of physics associated with strong fields. Even the experimental proof of the existence of the C-field supports this faulty understanding: the field measured by *Gravity Probe B* is incredibly weak, and this field is based on the mass of the Earth! That QGD is not *mass-based* so much as *mass-density-based* implies gravitomagnetism should be investigated in high density, strong field situations. This has meant, to most physicists, physics near black holes, however, the densest matter is not the black hole, but the elementary particle; the strongest fields are those found at the nuclear level of reality. Compare the mass density of the Earth at the distance of the *Gravity Probe B* satellite in 400 mile orbit to the density of fermions at atomic and nuclear distances.

Consider the relation of the electric charge of a particle to its density. Key is duality—Jefimenko [9] showed that Maxwell's electromagnetic equations and Heaviside's gravitomagnetic equations are *dual* if mass is constant (dual to charge):

$$\{q, \boldsymbol{E}, \boldsymbol{B}\} \asymp \{m, \boldsymbol{G}, \boldsymbol{C}\} \tag{7}$$

Mass is invariant [10], so Maxwell's equations have essentially the same solution as Heaviside's. Density-based duality implies that both are scale invariant from effectively zero to infinite scales, except for dimensioned physical constants: $g, c, h, \mu, \varepsilon$. If a scale exists where *both of the dual theories apply*, then charged particles arise from the C-field [11] leading to charge-based relations

$$\begin{bmatrix} q_e > q_u > q_d \\ m_e < m_u < m_d \end{bmatrix} \tag{8}$$

and Maxwell/Heaviside duality supports the evolution of the primordial field into particles, with the significant consequence that dual behaviors allow us to apply complex phenomena from electrodynamics to gravitodynamics, particularly solenoidal phenomena. Electrons trapped in Earth's magnetic field near the North Pole spiral down as the field grows stronger, emit radiation; massive particles can

become trapped in a strong $\boldsymbol{C}$-field, analogous with Maxwell since gravito-magnetic field $\boldsymbol{C}$ exerts force $\boldsymbol{F}=m\boldsymbol{v}\times\boldsymbol{C}$ on mass m causing the mass to follow a curved path. Applying Heaviside's law $\nabla\times\boldsymbol{C}\sim-\rho\boldsymbol{v}$ to each particle trapped in the field produces left-hand circulation of the C-field around the particles, adding to the environment surrounding the particle.

Figure 2 shows that the induced field inside the quark orbit is additive, increasing the field inside the orbit and hence tightening the orbit. Particles in orbit induce additive fields, strengthening the original external field $\boldsymbol{C}_{ext}$ that trapped the particles. The field induced by a local particle is labeled $\boldsymbol{C}_{ind}$. If two particles produce $\boldsymbol{C}_{ind}$, the strength of the induced C-field is $2\boldsymbol{C}_{ind}$. This is significant, since energy density of real physical fields, $\{E,B,G,C\}$, is proportional to the square of their field strength: $\left\{|E|^2,|B|^2,|G|^2,|C|^2\right\}$.

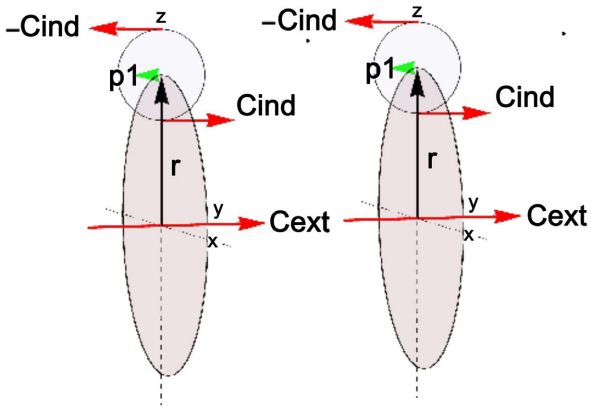

Figure 2. Two particles with momentum $\boldsymbol{p}_1$ induce C-field circulation with two induced components $\boldsymbol{C}_{ind}$ that add to the external field $\boldsymbol{C}_{ext}$ in which the two particles are trapped.

Hence two particles in adjacent orbits produce local field energy density $\sim 4C_{ind}^2$ and three particles in orbit produce local field $3\boldsymbol{C}_{ind}$ with local energy density $\sim 9C_{ind}^2$. The stronger field, $3\boldsymbol{C}_{ind}$, will tighten the orbit three times tighter than one particle-induced field and the tighter orbit will encircle *less* of the original external field, $\boldsymbol{C}_{ext}$, thus weakening the effect of $\boldsymbol{C}_{ext}$ while strengthening the combined effects of $\boldsymbol{C}_{ind}$. If the external field vanishes, can three captured particles remain entrapped? If so, the composite particle will continue to exist, potentially forever, physically explaining the existence of protons and neutrons in vacuum, where the original external field $\boldsymbol{C}_{ext}$ is effectively reduced to zero, after evolving from Big Bang to *now.* Immediately following the Big Bang, the density of primordial field ψ is assumed to be as strong as necessary to form fermions; most of the fermions formed in the universe were formed at that time and have lasted until now. We have a good idea of the energies involved in particle creation from particle colliders. Lacking an intuitively meaningful process, QED and QCD assume a *zero-point-energy* vacuum with *fluctuations* that give rise to virtual pairs of particles and antiparticles. If this energy existed, its mass equivalent would have

gravitational effects that simply are not observed in the universe and that yield approximately 120 orders of magnitude error between theory and measurement.

Qualitative description of the above physics is in "*Origin of strong force in quantum gravity*"; the model predicts phenomena such as the magnetic moment of the deuteron using simple math, compared to lattice QCD treatments based on 84 numbers at each lattice point in the calculation. Our goal for QGD is quantitative description of the dynamics of baryons: protons and neutrons, with up quark mass $m_u \sim 2.8\,\text{MeV}$; down quark mass $m_d \sim 5.2\,\text{MeV}$. Primordial field equations, based on Heaviside/Maxwell, are used to derive baryon dynamics.

To a first approximation, the problem is separable: *quark orbits* are assumed to induce the C-field necessary to self-capture, *i.e.*, to constrain the quarks in orbit, while *quark charges* attract quarks with opposite sign and repel quarks with like sign. In terms of Figure 1 quark orbits are responsible for the field that holds the quarks to *circle* about the z-axis. Electric forces cause orbits to *move* on the z-axis. The separation of charge and mass effects is only to 1st order. Generally speaking, the closer the orbits to each other, the stronger the combined induced C-fields; change in inter-quark-orbit distances due to charge will have effects on the strength of the flux tube, while any change in flux tube strength will affect orbital radii and thus have effects on inter-charge-distance. We solve for effects using separable mass and charge then attempt to analyze 2nd order effects in terms of these solutions via simplifying approximations. If we approximate each quark orbit as a coil or ring with equi-distributed electric charge, we can calculate force of the ring at a point on the z-axis, a problem long solved for electrostatics. The 3D electric charge problem reduces to a 1D approximation—appropriate since string theory was based on Veneziano's observation that proton collision dynamics produced behavior similar to that of string equations.

The 1D approximation for electrodynamic forces is known to be good at mid-to-large distance separation of the quark orbits, while degrading when orbits are very close. This is compensated by the fact that the gravito-dynamic forces are strongest when orbits are in close proximity, tending to overwhelm charge-based effects. The 1D approximation is conceptually string-like, more intuitive than 3D quarks constrained to orbits, and consistent with the inherent orbital nature of the flux tube architecture, wherein calculation of induced C-field via quark orbit symmetry based on any plane containing the z-axis intersecting the quark orbits at two locations, with momentum of the orbiting quark at these locations equal in strength and opposite in direction.

4. Calculation of Electromagnetic Quark Forces

The basic model of the quark in primordial field theory is based on solenoidal self-trapped quarks orbiting a common axis, a 3D problem to be approximated in one dimension. Considering quark orbits as equi-distributed charge on a ring, centered on the z-axis at z_i, allows use of Maxwell's electrostatic solution for the field at a point on the axis, formulated as

$$E(z)=\frac{q_i}{4\pi\varepsilon_0}\frac{z-z_j}{\left(r_i^2+\left(z-z_i\right)^2\right)^{3/2}} \tag{9}$$

Let $z_i=0$, in which case

$$\boldsymbol{E}(z)=\frac{q_i}{4\pi\varepsilon_0}\frac{z}{\left(r_i^2+z^2\right)^{3/2}}\hat{k}\,. \tag{10}$$

Next, I would like to scale q_i such that the charge on the ring, as seen at z on the axis, is equivalent to a point on the axis $q_i'=\kappa q_i$ and

$$\boldsymbol{E}(z)=\left(\frac{1}{4\pi\varepsilon_0}\right)\frac{q_i'}{z^2}\hat{k}\,. \tag{11}$$

Hence

$$\frac{q_i}{4\pi\varepsilon_0}\frac{z}{\left(r_i^2+z^2\right)^{3/2}}=\left(\frac{1}{4\pi\varepsilon_0}\right)\frac{\kappa q_i}{z^2} \tag{12}$$

solving for κ

$$\kappa=\frac{z^3}{\left(r_i^2+z^2\right)^{3/2}}=\left(\frac{z}{\sqrt{r_i^2+z^2}}\right)^3\equiv\cos^3\left(\theta_i\right) \tag{13}$$

Thus, the force on a charge q at position z on the Z axis, due to a ring at $z=0$ with charge q_i equally distributed on it, will be

$$F(z)=\left(\frac{qq_i}{4\pi\varepsilon_0}\right)\frac{\cos^3\left(\theta_i\right)}{z^2}\,. \tag{14}$$

This approach can be used to calculate the force between *two* coaxial rings on the z-axis at z_i and z_j with both rings approximated as points on the z-axis at z_i and z_j respectively. For each ring, *j*, assume that ring parameters q_j, m_j, r_j, z_j are unique, *i.e.*, the rings differ in charge, mass, radius and position on the axis. To do this I need another assumption: that the force felt by ring *j* at z_j due to ring *i* at z_i is equivalent to the scaled charge $q_j'=\kappa_{ij}q_j$ at a point on the axis at z_j. Thus, two scaling factors are needed as depicted in Figure 3.

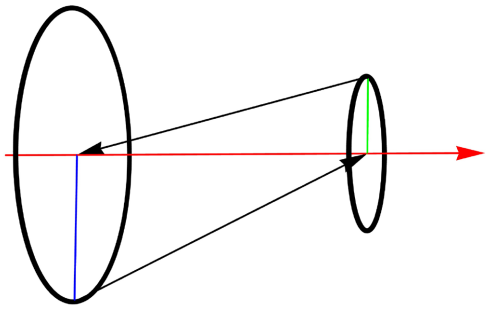

Figure 3. Illustrating the two angles θ_{ij} and θ_{ji}.

Finally, although the distance $\left(z_i-z_j\right)$ is the same (except for sign) for both

scaling factors, the relevant angle subtended by the ring depends upon the respective radius of the ring. That is, the force on ring j due to the charge on ring i is the function of the field at z_i due to the scaled charge q_i of ring i such that $q_i' = q_i \cos^3\left(\theta_{ij}\right)$ where θ_{ij} is the angle subtended by radius r_i. But this field will effectively act on the scaled charge q_j at z_j which, from the perspective of q_i' is scaled by $\cos^3\left(\theta_{ji}\right)$ where θ_{ji} is the angle subtended by radius r_j. Hence the force of q_i on q_j is

$$F_{ij} = \left(\frac{q_i q_j}{4\pi\varepsilon_0}\right)\frac{\cos^3\left(\theta_{ij}\right)\cos^3\left(\theta_{ji}\right)}{\left(z_i - z_j\right)^2}\operatorname{sgn}\left(z_i - z_j\right). \tag{15}$$

A procedure for iterative simulation of the dynamics of the rings used for three quark simulation of proton is based on *Duckworth* [12], the total force exerted upon the point charge q_j by n point charges is given by:

$$F_j = \sum_{i=1}^{i=n} F_{ij} = \sum_{i=1}^{i=n}\left(\frac{q_i q_j}{4\pi\varepsilon_0}\right)\frac{\mathbf{r}_{ij}}{r_{ij}^3} = \frac{q_j}{4\pi\varepsilon_0}\sum_{i=1}^{i=n}\frac{q_i \mathbf{r}_{ij}}{r_{ij}^3} \tag{16}$$

For the k^{th} particle

$$\textbf{If } (i = k) \text{ return, } \textbf{else } \left(\frac{q_i q_j}{4\pi\varepsilon_0}\right)\frac{\mathbf{r}_{ij}}{r_{ij}^3} \tag{17}$$

Based on the force formula for the three quark model of the proton, the analogous N-quark model potentially extends the model to tetra-quarks and penta-quarks. Summing over all $j \neq i$ gives the net force on ring i

$$F_i = \sum_{j\neq i}\frac{q_i q_j \cos^3\left(\theta_{ij}\right)\cos^3\left(\theta_{ji}\right)}{4\pi\epsilon_0\left(z_i - z_j\right)^2}\operatorname{sgn}\left(z_i - z_j\right). \tag{18}$$

The equations of motion then yield a set of coupled one-dimensional differential equations:

$$m_i\frac{\mathrm{d}^2 z_i}{\mathrm{d}t^2} = F_i. \tag{19}$$

Although each q_i' and q_j' depends on both rings' positions, the problem has now been reduced to a 1-D N-point system suitable for numerical simulation. As time evolves, $z_i(t)$ changes, and so do the angles θ_{ij}, ensuring that at each timestep the forces are recalculated correctly.

5. Calculation of Gravitomagnetic Quark Forces

The primary force responsible for capturing quarks in orbit is the Lorentz force of the strong gravitomagnetic C-field: $F = mv \times C$ assumed present post-Big Bang. For a local coordinate system with coaxial quark orbits in the xy-plane; if quarks are tightly bound to the external C-field and co-axial on the z-axis with Coulomb charged-based quark interactions affecting their z-position, can quarks stabilize for some arrangements? An up-quark will be attracted to a nearby down-quark, while another up-quark on the "other side" of the down-quark orbit will

be attracted to the down-quark but will repel the first up-quark. We test this u-d-u construction for stability for a given range of energies and parameters. The gravitomagnetic force of the strong field causes quarks to orbit; the quarks' self-induced fields will cause quarks to *spiral into* a tighter orbit, and hence to speed up or spin faster. Speed of the construct along the z-axis is arbitrary, assuming all quarks end up with approximately the same speed, however speed of the orbiting quarks in the xy-plane is not arbitrary but is assumed to approach the speed of light, as if a skater pulls her arms in to almost zero. At quark orbit dimensions, charges are treated as *smeared over* the orbit—*i.e.*, as charged *rings* with equi-distributed charge on each ring. Rather than quarks individually free to move in three dimensions the model assumes three co-axial rings in the xy-plane, separated along the z-axis, with the C-field preserving ring geometry, with Coulomb field interaction dynamics along the z-axis. We calculate C-field energy at point $\boldsymbol{x}_i$ from momentum density $\boldsymbol{p}_j$ using the Heaviside-derived equation

$$\boldsymbol{C}_{ij} = \boldsymbol{x}_i \times \boldsymbol{p}_j \tag{20}$$

Calculating the C-field at any such point allows a sequence of points or a path to be defined for multiple sources, specified at a given time.

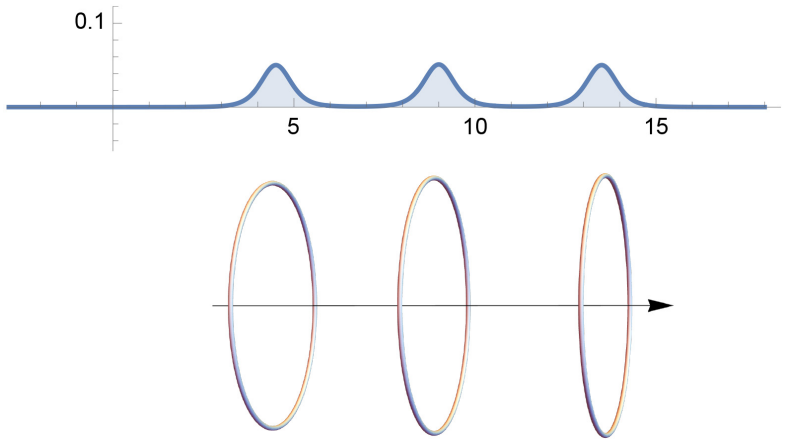

Figure 4. The C-field energy density for three coaxial quark "orbits" on the axis of symmetry.

If quark orbits are sufficiently separated, the left-handed circulation induced by the momentum at any point on a quark orbit will cancel the induced circulation from momentum at the same point on an identical neighboring quark (**Figure 4**) and C-field energy density midway between the coaxial quark orbits vanishes. As quark orbits approach each other on the common axis the on-axis C-field energy density increases, as indicated by the filled in area under the curves. This gravitomagnetic analog of electrical currents in loops inducing a coaxial magnetic B-field implies that we can bring the coils closer together to achieve a solenoidal effect. Key to solenoidal physics: the contribution to the common field from N current loops is increased over that of one current loop by a factor of N and since energy density is proportional to the square of the field, the energy density is increased

by N^2. The gravitomagnetic fields in the analogous *solenoids* are represented in three energy density diagrams in Figure 5. The figure is not to scale; 10 units on the horizontal axis correspond to approximately one femtometer, ~10^{-15} m.

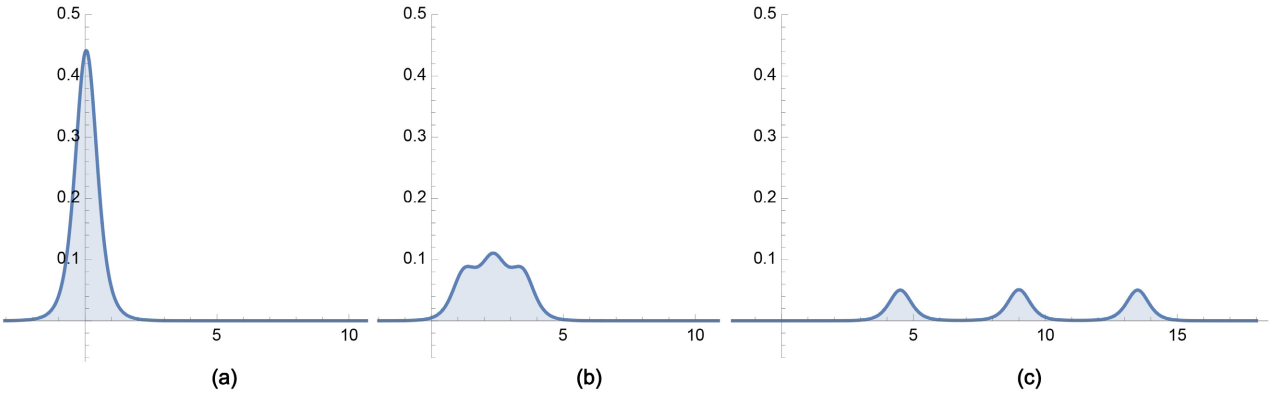

Figure 5. The *solenoidal* effect of bringing quark orbits closer together.

This energy-dependent construction can be disrupted by sufficient energy input to the system by external particles; in which case the phenomenon of *quark confinement* follows from the model. The Lenz-like response of a disturbed C-field is such that the collapsing field generates sufficient local *gmf* (gravitomagnetic analog to *emf*) to occasion particle pair creation, producing a ***replacement* quark** for the one "knocked out" of the system and an **antiquark**, that pairs with the knocked out particle and thus forms an escaping meson.

Figure 6 represents local C-field density at u-d-u locations on the axis based on varying the orbital radii. Conversely, orbital radii are based on local C-field values.

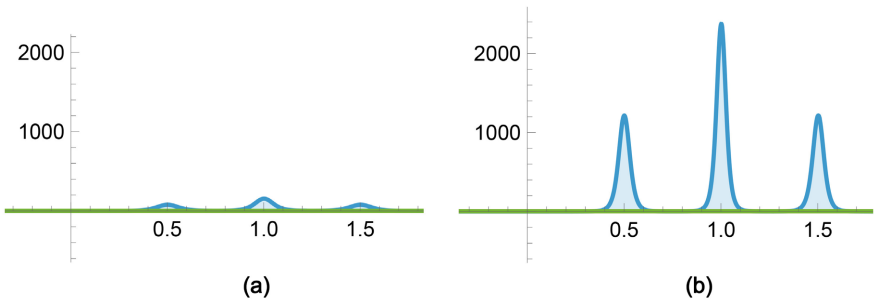

Figure 6. Example dependence of C-field energy density on orbital radii.

Strength of the field induced by the momentum of the quark in orbit is based on the distance from the z-axis—the value of the orbital radius. The Lorentz force bends the quark into a tighter orbit for a stronger external C-field, where tighter orbit means a smaller radius. Hence, the radius affects the strength of the coaxial field induced by any quark, and the strength of the coaxial field affects the radius of the orbit in which the quark is captured. Lefthand Figure 6(a) represents a radius value 1.0, while righthand Figure 6(b) has a radius value ~0.5. Halving the radius doubles the C-field strength, hence quadruples the energy density of the

field, as is approximately shown in the figure. The Lorentz force equation contains the mass of the particle upon which the force is acting, so the more massive down quark will be expected to occupy an orbit with a tighter radius than that of an up quark. The down-quark in the center has a smaller orbital radius, since the mass of the down quark is approximately twice that of the up quark, hence the larger down quark C-field energy in Figure 6. The 3D-to-1D treatment of the charged quark *ring* is strongly a function of the quark orbital radius of the *ring* as is seen from the $\cos^3$ term: $\kappa = \dfrac{z^3}{\left(r_i^2 + z^2\right)^{3/2}}$.

Strength of the local C-field is dependent on the quark orbital radius, and a factor of specific quark mass and velocity. The radius of the specific quark orbit is dependent on the strength of the local C-field that produces the Lorentz force causing the quark to orbit the local field. Inter-quark spacing along the coaxial z-axis is affected by the electromagnetic field approximated as a one-dimensional problem, and the inter-quark spacing determines the strength of the C-field energy density as shown in Figure 5. In Figure 5(a) the C-field is strongest when inter-orbit spacing is smallest. This brings another dependency on degree or degree of freedom into play.

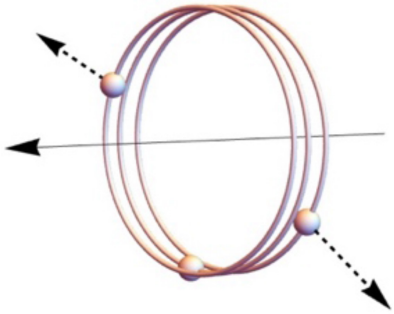

Figure 7. Adjacent orbits of like quarks exert little or no axial electric force but instead produce outwardly directed radial forces, potentially modified by unlike quark charges in the vicinity.

Two orbits occupying almost the same intersection with the axis have little or no coaxial electrical force; there is however an associated radial force (Figure 7). For almost-coincident up quark orbits, the quarks will repel each other radially. This counteracts to some degree the shrinking of the radius occasioned by the intensified C-field due to the accompanying decreased orbital separation, probably further stabilizing the system but certainly complicating hadron dynamic calculations. This multidimensional radial dependence of the model clearly precludes any simple linear QGD analytic solution of the hadron model dynamics!

In Figure 8(a), three quark orbits have initial x-axis positions: x_1, x_2, x_3, shown vertically. We vary the orbital separation over time with x2-x1 and x3-x2 beginning at zero and growing linearly over time, which varies from zero to 500 time units on the horizontal axis. The C-field containment force at zero orbital separa-

tion is zero, rapidly grows to a peak, then decays as the quark orbits move away from their solenoidal grouping, per Figure 8(b). The leftmost quark position x1 is shown blue, the central down quark at x2 is orange, the rightmost up quark position x3 is green.

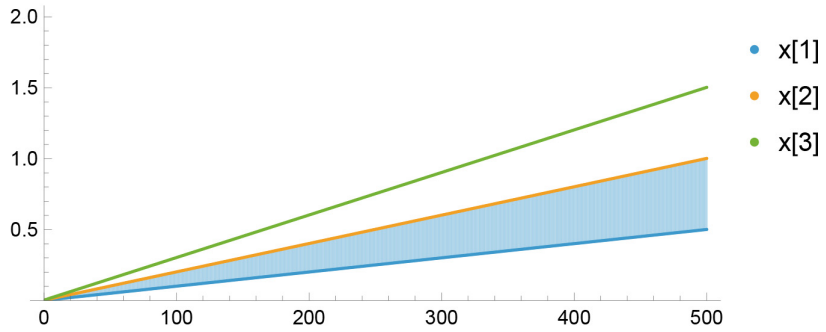

(a)

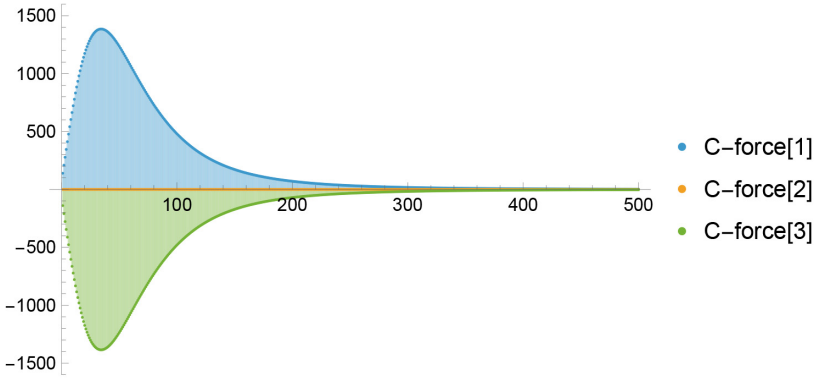

(b)

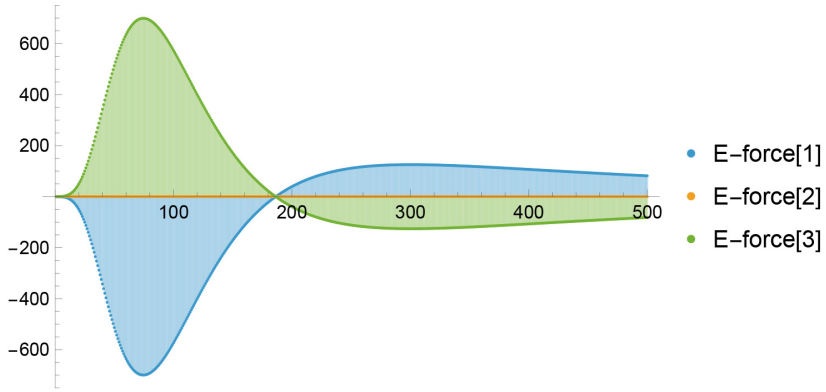

(c)

Figure 8. (a) x1, x2, x3; (b) C-force [1, 2, 3]; (c) E-force [1, 2, 3].

In Figure 8(b), the blue force of the C-field on the left up quark is positive, acting to move the quark in the positive direction toward the other two quarks. The green force on the right up quark is negative, acting to move this quark in the negative direction toward the other two quarks. With initial symmetry the orange force on the down quark is balanced, hence the force is zero. The forces are calcu-

lated consistently, but not to scale; at this point the actual hadron quark density, the amplitude of the orbital radii, and the inter-orbit separation are all unknown, so arbitrary scale units are chosen for convenience. In Figure 8(c), the blue force of the electric charges acting on the leftmost up quark is negative, acting to push the leftmost quark away from the other two quarks, in spite of the fact that the nearest quark, the down quark, is oppositely charged and would be expected to attract the up quark. The electric force is proportional to the product of charges:

Force between the left up quark and the down quark is proportional to:

$$\left(\frac{2}{3}\right)\left(\frac{-1}{3}\right)=\left(\frac{-2}{9}\right).$$

Force between the left up quark and right up quark is proportional to:

$$\left(\frac{2}{3}\right)\left(\frac{2}{3}\right)=\left(\frac{4}{9}\right).$$

Based on charges, the up quark repulsion can dominate up-down attraction; however, electric force also depends on the distance between orbits, and the left and right up quarks are initially twice as far apart as either is from the oppositely charged down quark. As the distance between the orbits increases, the outer quark forces become weaker compared to the force between either of the outer quarks and the central down quark. At some point the forces equate and beyond this point attraction between up and down quarks dominate repulsion between up quarks. In Figure 8(c), this point occurs at time ~188 and the corresponding inter-orbit separation from Figure 8(a) is ~0.19.

The green force on the right most up quark is, of course, equal in magnitude and opposite in direction. The orange electrical force on the central down quark is balanced, hence zero. Although the orange force remains zero, in time the blue and green forces change polarity, since the forces are not only proportional to charge, but also inversely proportional to the square of the separation distance. When the particles move far enough away, the force from the very far up quark is negligible with respect to that from the central down quark, and the force becomes attractive, acting to pull the two up quarks back toward the down quark. The scales used in these calculations are chosen for convenience and the use of color is for identification of curves and has nothing to do with QCD "color". The 1D approximation for handling the charge on the quarks depends upon the angles involved; when two orbits are extremely near each other the cosine of the angle is almost zero and the cosine cubed terms effectively make the forces vanish. This is worsened by the use of constant radii in our current treatment. Nevertheless, the force curves shown in Figure 8 describe the key features of hadron dynamics.

Figure 9 displays instances of the strong C-field force as a function of quark separation. Figure 9(a) shows the shape of C-field energy density on axis of proton solenoid, when quarks are very closely grouped and C-field energy density is peaked. Horizontal lines depict values of the C-field force acting to confine the quarks. Due to symmetry, the force acting on the down quark at center is balanced; the green line overlying the x-axis shows that zero force acts on the down quark. The orange line at $y=+40$ represents the large positive force on the leftmost (up)

quark pushing the quark to the right (in the positive x direction) while the red line at $y=-40$ represents negative force on the rightmost (up) quark pushing the quark to the left (negative x direction). In Figure 9(b), quarks spread out more; both local energy density (under curve) and associated C-field force are reduced. In Figure 9(c), quark separation increases with consequent C-field effects decreasing, and Figure 9(d) shows the three quarks effectively separated with no strong force acting to keep them together.

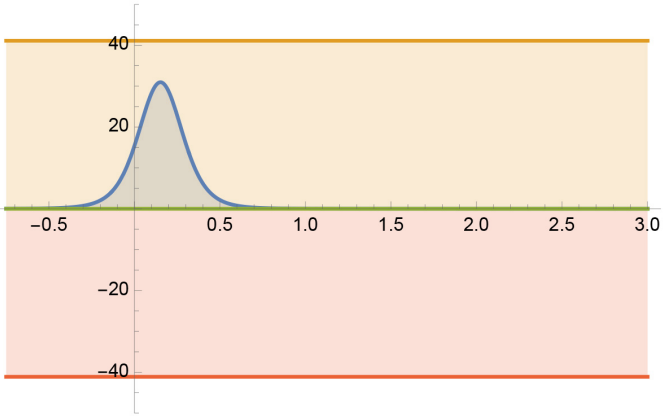

(a)

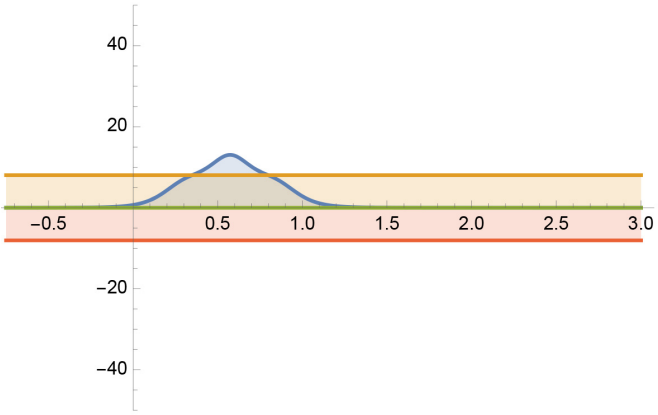

(b)

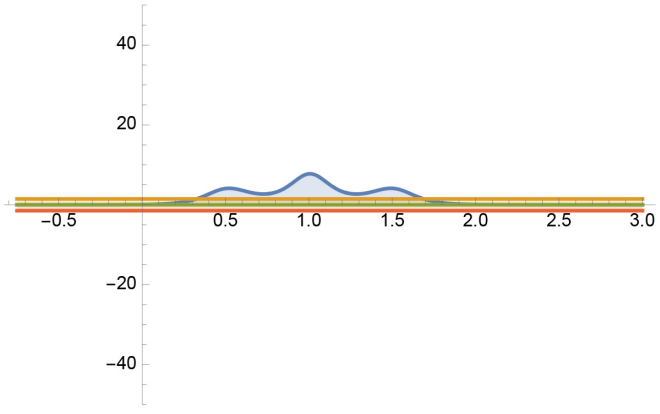

(c)

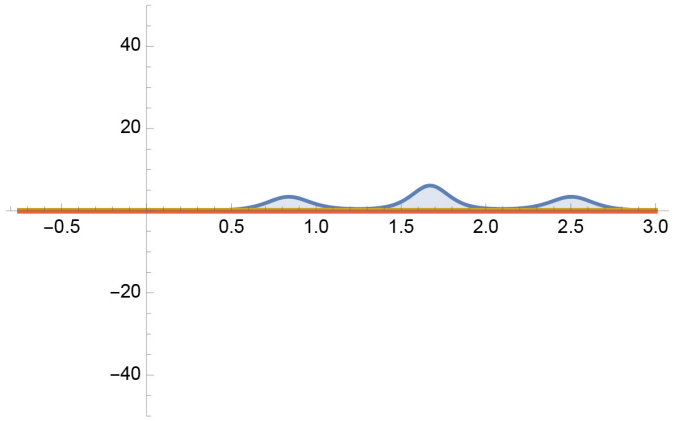

(d)

Figure 9. C-field forces as function of quark orbital separation.

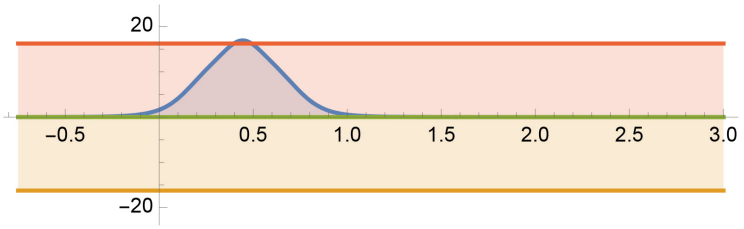

(a)

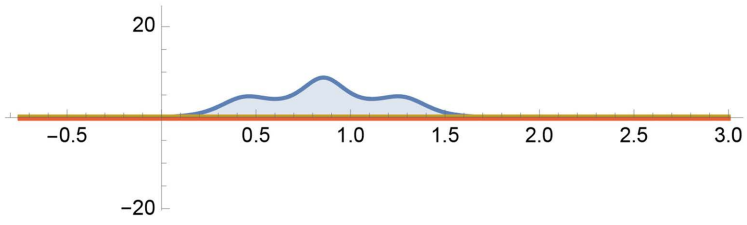

(b)

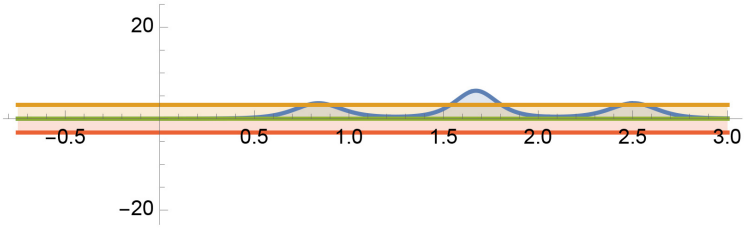

(c)

Figure 10. E-field force as function of quark separation.

Figure 10 displays examples of the electric E-field force as a function of quark separation and E-field strength. The peaked curves still represent induced C-field energy density, but the horizontal lines now depict E-field forces acting on the quarks. Due to symmetry, E-forces on the down quark are balanced, represented by the green line at $y = 0$. The orange line at $y \approx -18$ represents negative force on the leftmost up quark pushing the quark to the left (in the negative × direction)

due to the fact that the positive charge on the rightmost up quark exceeds the negative charge on the down quark. The red line at $y \approx +18$ represents the positive force on the rightmost (up) quark pushing the quark to the right (in the positive x direction). Thus, as shown in these two figures, the electric forces tend to push the quarks apart, while the gravitomagnetic forces tend to confine the quarks in a tight grouping. The E-forces depend on both charge and distance, with the charge unchanging. As the distance between quarks varies the force varies and as shown in Figure 10(b), the forces become balanced at one distance. Finally, as the quarks move still further apart (Figure 10(c)) the higher charge on either up quark is relatively weaker than the oppositely charged down quark and the forces on the up quarks now reverse, tending to attract the up quarks back toward the down quarks, as indicated by the fact that the red line is now below the x-axis and the orange line above.

Quark charges are known, and quark masses are known approximately, depending on the scheme being used to determine the quark mass; they are never individually measured. In a time-based simulation, the time-step size is scaled by an arbitrary ***tscale***. Since the actual mass densities of the quarks are not yet known, we provide a scale constant ***kf*** to multiply the quark mass terms. The density-dependent parameters, such as the C-fields and the orbital radii are also unknown. A scale constant ***kc*** is used to scale the C-field force and a scale factor ***kr*** is used to scale the radii. Since the 1D electrical force approximations depend upon quark orbital separation distances (for each simulation run) and the orbital radii, a scale constant ***ke*** is used to scale the electrical force. The actual values of the parameters are unknown, but the relationships are defined by the QGD model as described above and previously. The hadron problem then becomes that of finding stable solutions, *i.e.*, solutions in which the hadron configuration retains its integrity. If such can be found, the problem then becomes that of showing that actual physical data measurements support the range of scale parameters that produce stability. Based largely on the duality with electro-dynamical problems, the gravito-dynamic problems are intuitively comprehensible. It remains to be seen whether the QGD model can match the hadron data obtained in colliders. The above forces have been calculated by ranging over specific inter-orbital separations, not by dynamically calculating these positions, which we do in the next section.

6. Calculation of Gravito-Electro-Magnetic Quark Orbital Dynamics

The C-field and E-field forces acting on quarks in the above examples have been evaluated separately, with scalable amplitudes. Calculations have been essentially static, with the simulation system driving inter-orbital separation and forcing the radii of the orbits. In most cases radii are held constant while orbital separation is varied. The cases in which the orbital radii are varied based upon the strength of the C-field determined by orbital separation have tended to blow up. As seen, a significant amount of insightful information has been derived from this forced

approach. In contrast to this essentially static approach, in a real hadron the C- and E-forces act on all quarks all the time and determine the internal dynamics of the composite particle, based on time-based positions, velocities, and forces for quarks constituting a hadron.

Whereas *QGD lattice dynamics* are involved in generating fermions, hadron dynamics are simply Newtonian physics, augmented by Heaviside. Forces are calculated given quark id and position vectors, then force equations are solved and the position vectors updated. The following algorithm is used to compute the QGD dynamics of the hadron.

7. The Nucleon Algorithm

Begin:

Calculate the C-field at x_1 on the x-axis, the center of the first up-quark orbit, from the 6 momenta where the quark orbits intersect the $z=0$ plane, using $\boldsymbol{C}_{ij}=\boldsymbol{x}_i\times\boldsymbol{p}_j$. Similarly, calculate the C-field on the axis at x_2 and x_3 due to the 6 momenta.

Calculate the C-field energy density at x_1, x_2, x_3: $\left|\boldsymbol{C}\cdot\boldsymbol{C}\right|$.

Using these three values of *C*, recalculate the radius: $r_i=\dfrac{1}{C_i}$ where speed of light $c=1$.

Based on these 3 radii, map the three charged quark orbits onto the x-axis as scaled point charges, and calculate the force on each scaled charge point from the other two scaled charged points. Based on the quark masses, solve for the velocity of each quark "point" (in 1D) using

$$eForceOn\left[i\right]=\sum_{j\neq i}\frac{q_iq_j\cos^3\left(\theta_{ij}\right)\cos^3\left(\theta_{ji}\right)}{4\pi\epsilon_0\left(z_i-z_j\right)^2}\operatorname{sgn}\left(z_i-z_j\right)$$

We calculate C-field z-axis force, $cForceOn\left[i\right]$, based on energy density using the formula for change in work: $\mathrm{d}W_i=\boldsymbol{F}_i\cdot\mathrm{d}\boldsymbol{x}_i$ due to forces at each point. This is done by computing the field at each orbit-position $\boldsymbol{x}_i$ and determining the change in field at $\boldsymbol{x}_i\pm\mathrm{d}\boldsymbol{x}_i$. Then Equation (19) is invoked to yield a set of coupled one-dimensional differential equations:

$$m_i\frac{\mathrm{d}\boldsymbol{v}_i}{\mathrm{d}t}=\sum cForceOn\left[i\right]+eForceOn\left[i\right]$$

Then, for a given time step $\mathrm{d}t$, calculate the new positions x_1, x_2, x_3 of the quark orbits on the x-axis. (or z-axis per treatment chosen)

Repeat from **Begin**.

A sample simulation has a first up quark initially at position x1 = 0.45, the down quark at x2 = 0.9 and the third (up) quark at x3 = 1.35 with zero relative velocities at time zero. Scaling constants are chosen to produce the behavior of **Figure 11**, with zero initial orbital separation velocities.

Ability to obtain an oscillating solution from initial conditions is encouraging,

suggesting that the model is operating somewhat as expected. Nevertheless, anyone who has simulated Newtonian physics knows that this picture is not typical. A typical simulation picture is Figure 12, where stable behavior ceases, and symmetry is broken; energy has been added to the figure in yellow.

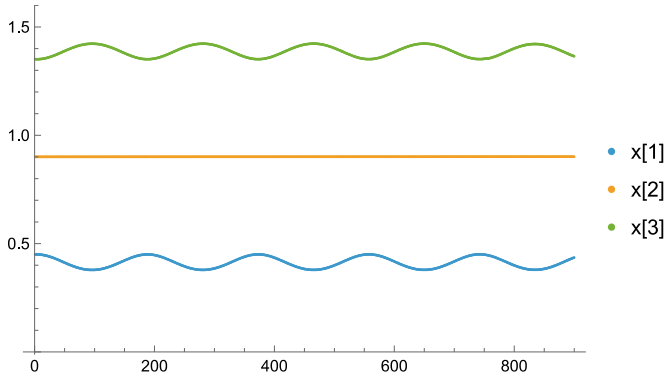

Figure 11. Time traces of axial positions of quarks 1, 2, and 3.

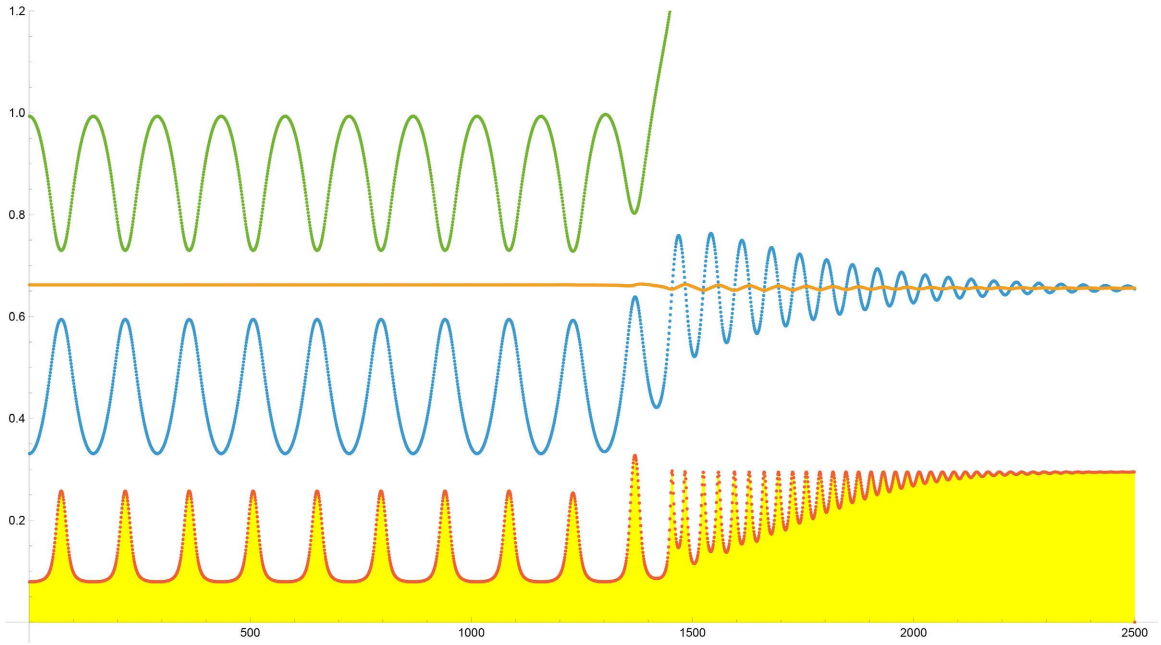

Figure 12. Scaling parameters: kx = 0.331, ke = 96, kc = 11.5. Up quark orbit x1 (blue) begins at position 0.331, down quark orbit x2 (orange) begins at 0.662, and up quark orbit x3 is placed at 0.993, then the quarks are released and the interactions used to obtain the orbital motions. As seen at about 1400 on the time axis up quark 3 is repelled by up quark 1 whose orbit approaches the down quark orbits and begins oscillating about the position of the heavier particle. The bottom curve, filled with yellow, shows the energy density of the system calculated at the x1 orbital position as a function of the dynamics; it peaks when three quarks are at closest approach, then decreases as the quarks move apart. In the end phase the up quark and down quark pair are expected to be unstable but may closely couple such that the solenoidal gravitomagnetic energy density is temporarily maximum.

8. Rethinking Aspects of the QGD Hadron Model: Mass and SU(3) Symmetry

Experience with this hadron model leads to reconsideration of several of the

original arguments concerning the QGD model. The model approximates a 3D charged quark as a 2D ring of charge and projects this as a point on the common axis to find the electric field at another point from the common axis where a second orbital plane intersects the axis. The force equations use the mass of the quark to move the quark orbit positioned at the axis, but possibly the angular momentum (of the C-field) of the quark orbit should be the basis of the relevant mass, as the quark orbit is the object being moved by the electrodynamic force. In one sense, this mass should be 1/3 of the mass of the hadron, *since it is the source of the hadron mass* [spin = mass]. If so, this should be used for the C-field force, or an inertial equivalent. We may have allowed this already via kf = *force constant*, which is basically a mass multiplier, thus requiring little modification of the model. The initial symmetry consideration may require a more significant rethink. The problem pre-QCD was that the Pauli Exclusion Principle required an anti-symmetric wave function, while the wave function was symmetric. Per Kerson Huang [13]:

> In a simple model, one puts the quarks into orbitals in a central potential, like electrons in an atom. Experiments show that the magnetic moment of a nucleon is close to the sum of quark magnetic moments. This suggests that all three quarks are in the lowest orbital; but this is impossible for they have spin 1/2 and should obey the Pauli Exclusion Principle. The way out is to endow them with a new attribute, so the quarks are not identical.

In 1964 O.W. Greenberg *proposed* color as this new attribute; this is the genesis of color; there was no other evidence of its existence. As an alternative, I initially proposed quark orbit position along the z-axis of the C-field flux tube to which the quarks are bound such that an anti-symmetric wave function based on the flux tube axis can label quark states. Assume a particle on either end remains on the end, with down quark separating the two up quarks, *i.e.*, assume the z-ordering is stable. Such a z-order wave function can be written:

$$\begin{aligned}\psi(z_1,z_2,z_3) = {} & \psi_1(z_1)\psi_2(z_2)\psi_3(z_3) - \psi_1(z_2)\psi_2(z_1)\psi_3(z_3) \\ & + \psi_1(z_2)\psi_2(z_3)\psi_3(z_1) - \psi_1(z_1)\psi_2(z_3)\psi_3(z_2) \\ & + \psi_1(z_3)\psi_2(z_1)\psi_3(z_2) - \psi_1(z_3)\psi_2(z_2)\psi_3(z_1)\end{aligned} \tag{21}$$

The Pauli Principle is satisfied: if we set $z_1 = z_2$, $z_1 = z_3$ or $z_2 = z_3$ the wave function becomes zero; there is zero probability of any two quarks sharing *the same orbit* at location z_i and *color* solves a non-existent problem. Experimentation with the hadron model has led to an appreciation that quark-orbits are not entities described by such wave functions, but dynamic configurations that can pass through each other moving in opposite directions. Dynamic forces become more complex, but Pauli is still satisfied—when quark orbital positions cross each other they move in opposite directions and thus are not identical. Nor, since the position of the quark *in* its orbit about the flux tube is unknown, can they be assumed to be identical. Thus, Pauli is not a problem in the flux tube model, but hadron dynamics becomes more complex. **Figure 13** shows simple orbit crossing

with orbits initially 0.331 distant from each other, and down quark at $x = 0.662$ on the common axis.

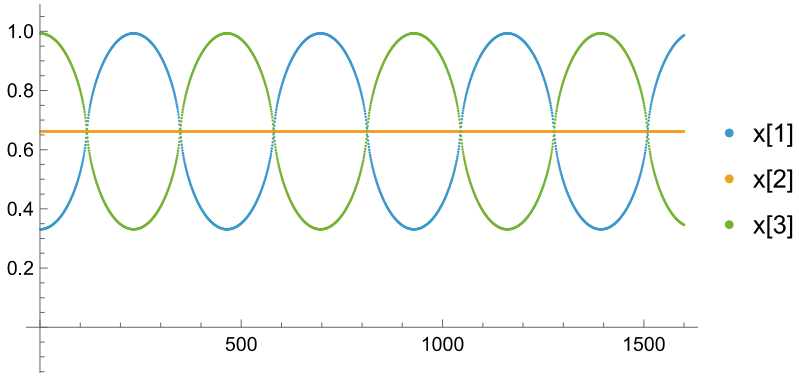

Figure 13. kx = 0.331, ke = 30, kc = 30.

Here symmetry is such that the outer up-quarks are forced toward the down quark, and cross paths at the position of the down quark, then experience a restoring force. This is not an exact solution since we consider constant radii for the orbits. The 1D approximation implies that the relevant cosine approaches zero when the z-axis distance approaches zero while the radius remains finite. At the exact position of crossing the electric field on the axis is zero, then the direction of the field reverses. From this perspective, orbital dynamics in **Figure 13** seem reasonable, but when we run this simulation for a longer time new behavior appears, as seen in **Figure 14**.

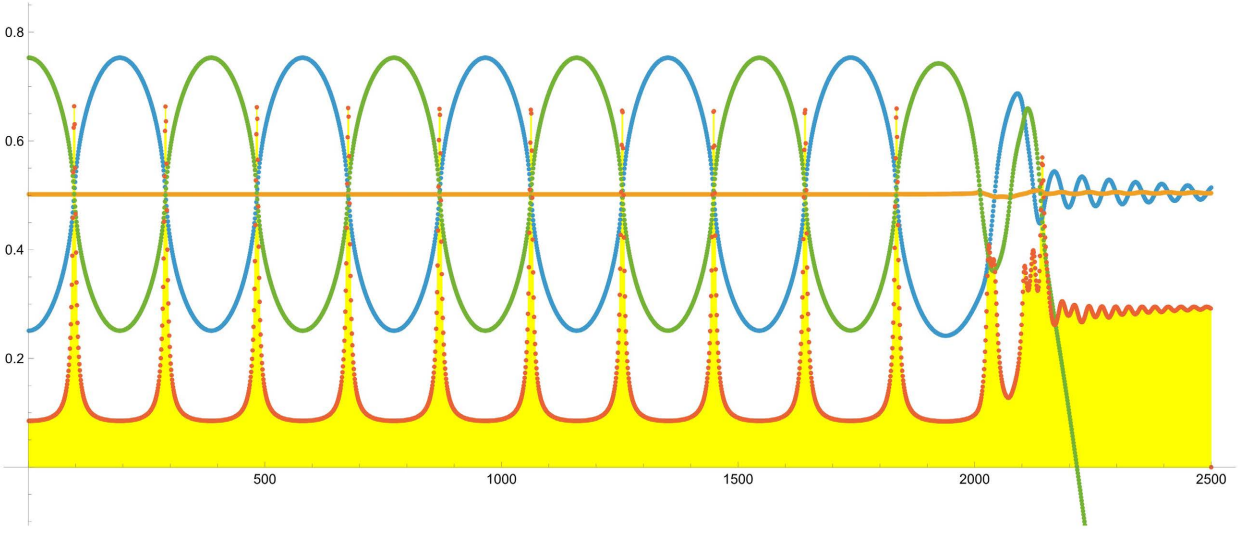

Figure 14. The C-field calculated at x1 position, shaded in yellow, grows large when particles approach each other extremely closing as at orbit-crossing points (kx = 0.251, ke = 10, kc = 10).

Quark orbits oscillate on the common axis as shown in **Figure 13** for the first 2000 time ticks. The C-field energy curve, scaled for convenience, is calculated at the x1 orbital position, filled in yellow, growing solenoidally when orbits approach

each other and shrinking accordingly when they move apart. Here up quark orbit x3 executes ten orbit crossings then becomes unstable and moves along the axis away from the other two quark orbits. As a result, up quark x1 is no longer repelled strongly by departing up quark 3 and moves in tightly to bind closely with down quark orbit x2. The average separation is much less, so according to the solenoidal physics the corresponding C-field energy, shown in yellow, is higher. By comparison, the yellow-filled C-field energy density curve does not grow in Figure 15 as it did in Figure 14, because the C-field is being calculated at quark x1's orbit position. In Figure 14, green orbit x3 moves away from the others after which up quark x1 binds more closely with down quark x2, providing solenoidal increase in C-field energy density.

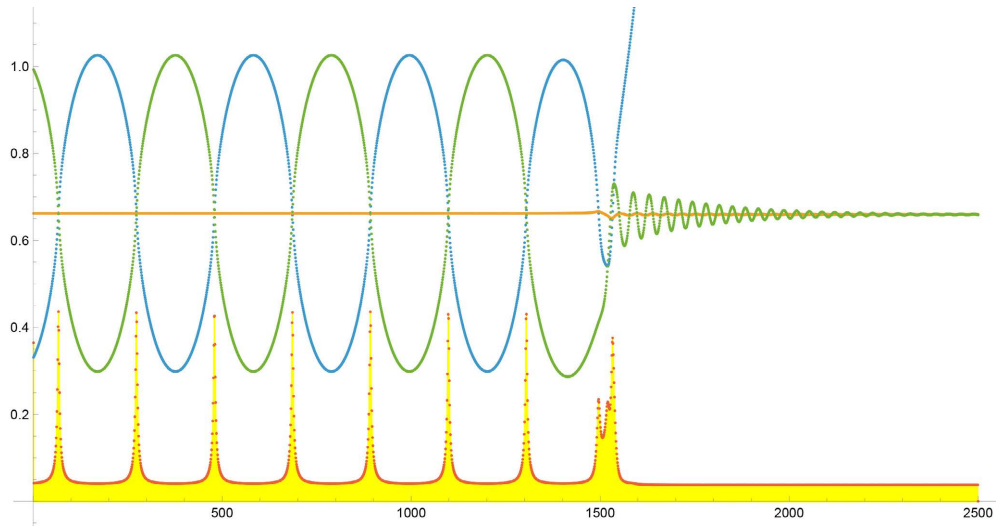

(a)

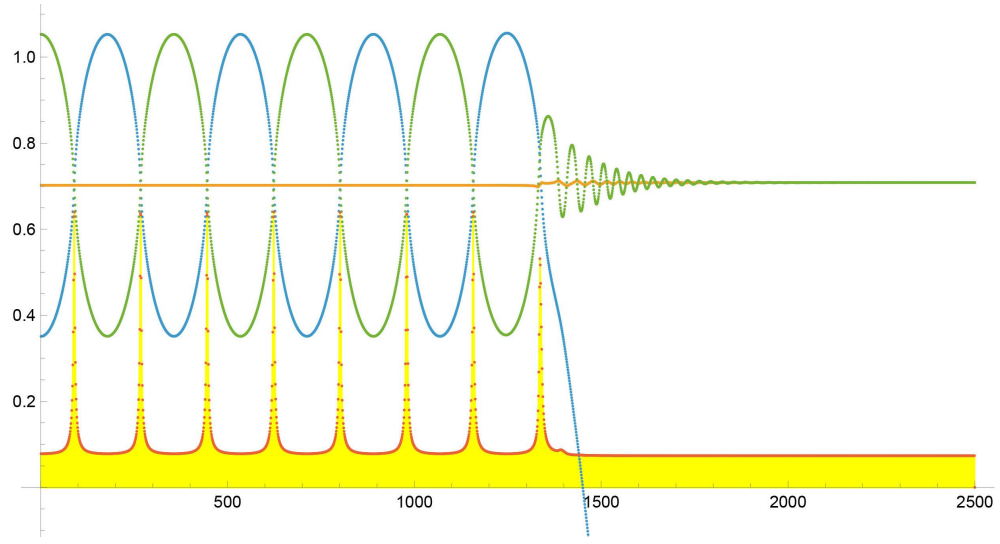

(b)

Figure 15. Simulation parameters: (a) kx = 0.331, ke = 30, kc = 30. (b) kx = 0.351, kc = 30, ke = 30. In both figures the C-field calculated at x1 position, shaded in yellow, grows large when particles approach each other extremely closely as at orbit-crossing points.

In Figure 15, blue orbit x1 moves away from the others and green up quark x3 then binds closely with orange down quark x2, providing the solenoidal increase. But C-field energy is still associated with the axis position of orbit x1, which has departed the other two quarks and does not see their solenoidal increase. In both cases we might expect the departing particle to produce a "jet" of quark-antiquarks and exhibit confinement. That is of course our end goal, but we are just beginning to simulate our gravitomagnetic hadron model and are trying to physically interpret what we see.

9. Quantum Gravitodynamics

Figure 16 shows orbit x1 position and combined gravito- and electro-dynamic force f1 acting on x1 and velocity v1 of the x1 orbit on the z-axis. The combined force acting on orbit x1 is

$$\mathrm{f1} = \mathrm{kc} * cForceOn(1) + \mathrm{ke} * eForceOn(1) \tag{22}$$

That is, the gravito- and electro-dynamic forces are calculated and scaled by constants kc and ke. The same calculations are performed for quark orbits x2 and x3 and the dynamics computed based on these forces. The remainder of this paper will investigate various dynamical configurations.

Plots such as Figure 16, for all quark orbits, potentially combine with C-field or E-field data allow for quite complex representations of the simulated dynamics, examples of which are shown in Figure 17. One can expand and interpret diagrams to identify the dynamics that proceed in the simulation.

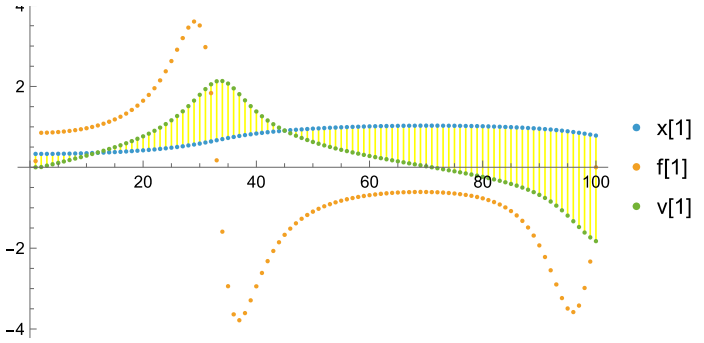

(a)

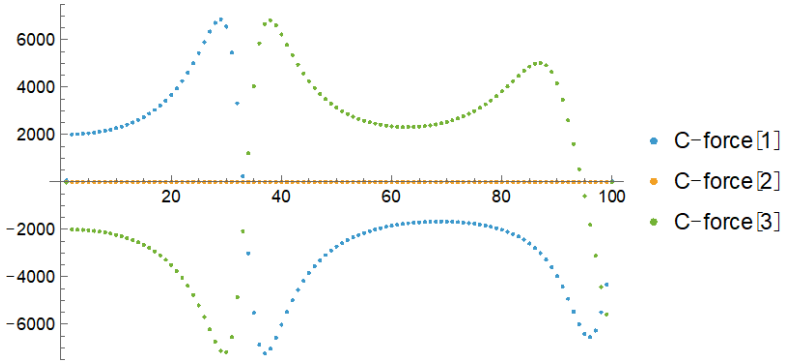

(b)

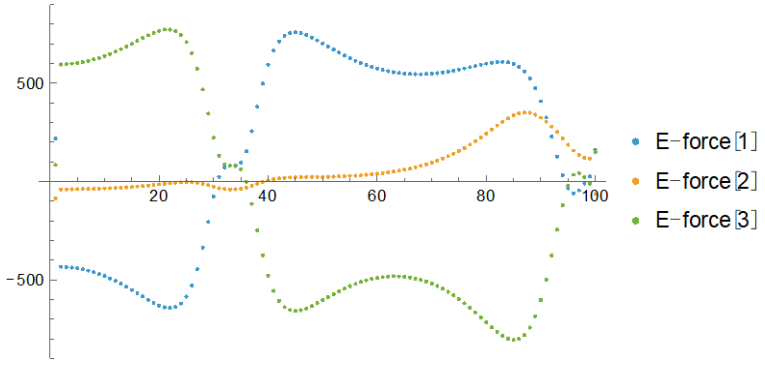

(c)

Figure 16. (a) Combined force f1 acting on orbit x1 and velocity v1 of the orbit on the z-axis. (b) C-field forces acting on each quark orbit. (c) E-field forces acting on each quark orbit.

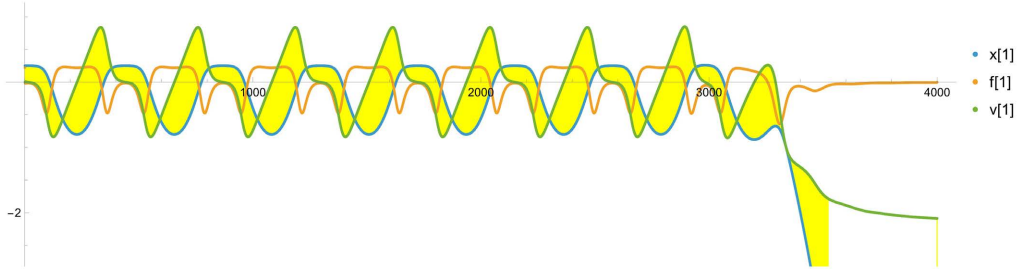

(a)

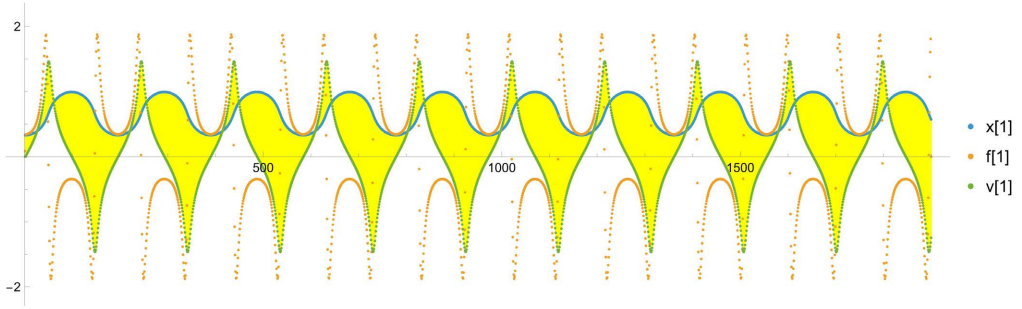

(b)

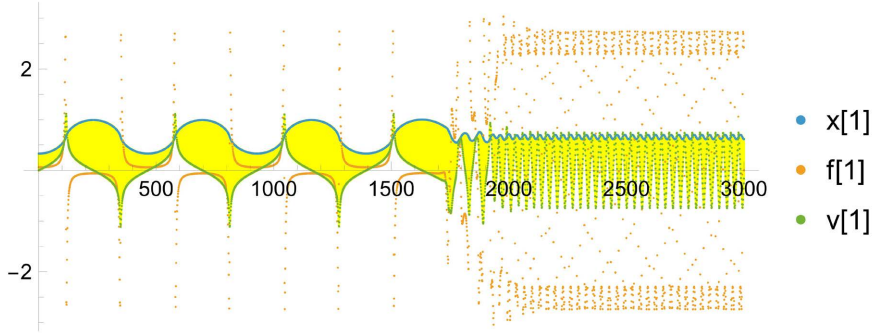

(c)

Figure 17. (a), (b) and (c): Displaying force f1 acting on orbit x1 and velocity v1 of the orbit on the z-axis for different values of the scaling constants kc and ke. Combined with energy, quite complex displays present information on hadron model simulation dynamics, mostly useful for debugging.

Curves in Figure 17 illustrate complexity and are useful for debug, but little else. They demonstrate that the simulation is quite robust, a key result of this paper. Our goal is to analyze quantum gravito-dynamics QGD and build a simulator to investigate the model. Multi-parameter displays are good for exploring parameter interactions and debugging, but the primary information is derived by tracking quark orbits positions, x1, x2, x3 over time as shown for selected time slices in Figure 18.

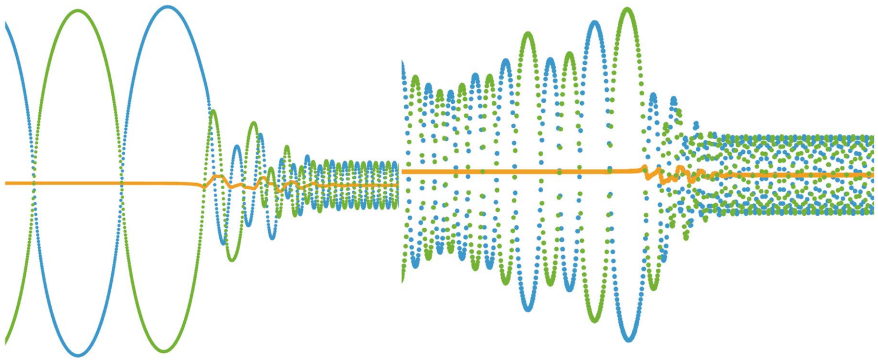

(a) (b)

Figure 18. (a) and (b) Typical time-slice diagrams of quark orbits, x1, x2, x3 over time.

In Figure 18(a) and Figure 18(b), the down quark orbit, x2, shown in orange, is balanced by the symmetry of the x1 and x3 orbits until disturbed by an instability, at which point the down quark orbit becomes unbalanced and behaves accordingly. In both cases, rather than one quark escaping, all three quark orbits settle into a new stable equilibrium and balance returns.

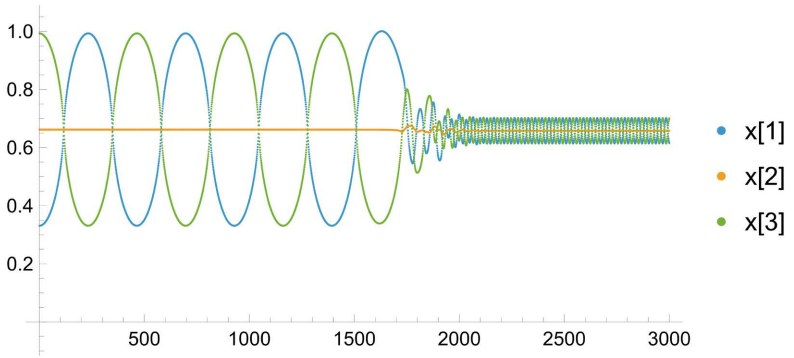

Figure 19. Quark orbits, x1, x2, x3 for force parameters: kx = 0.331, ke = 30, kc = 100.

Figure 18(a) shows a time slice from the Figure 19 diagram, depicting an initial quark separation 0.331, which oscillates for eight crossings, then switches to a more stable behavior in which up quarks oscillate between 0.614 and 0.702 while the down quark remains stable at 0.658 with a maximum inter-orbit separation of 0.044, confined by the strong gravitomagnetic force. Next, we retain these force constants but begin with initial orbital separations approximately one half that of

Figure 19. The result, a slice of which is represented in Figure 18(b), is shown in Figure 20 for an extended period of time.

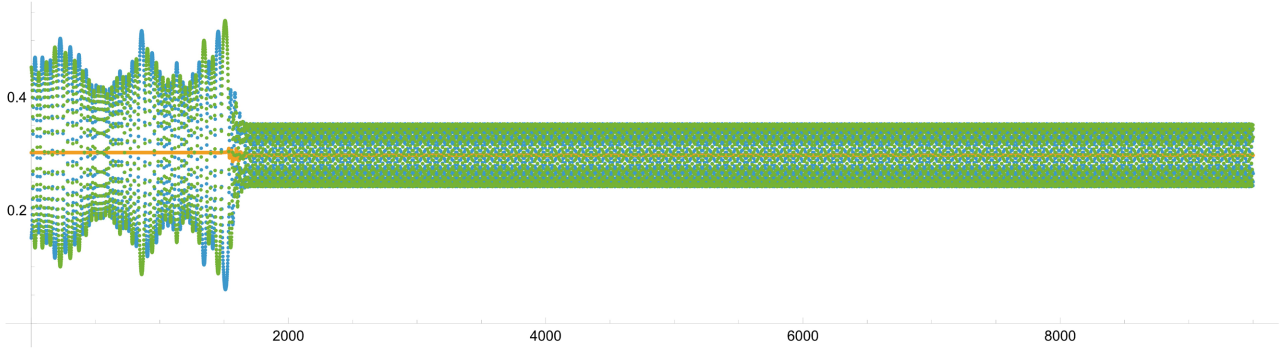

Figure 20. Proton quark orbits x1, x2, x3 for force parameters: kx = 0.151, ke = 30, kc = 100.

In Figure 20, inter-orbit separations range from about .104 to .233 executing a number of oscillations in which orbits cross on the z-axis. After an instability triggers an asymmetry, separations reduce to .055 units, with increase in C-field flux tube energy density, as seen in Figure 21. This state appears to be very stable, although we show only about 10,000 time steps in Figure 20, although the model runs to at least 100,000 times steps with no changes in stability.

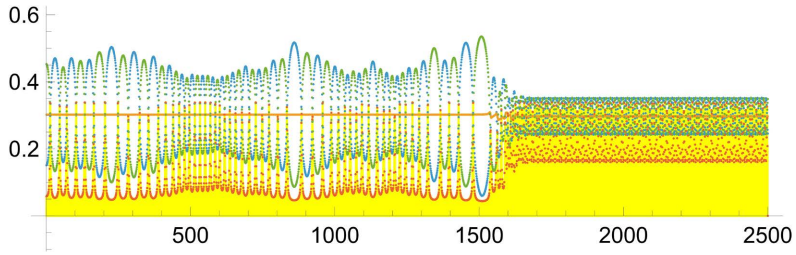

Figure 21. Energy diagram for proton dynamics: kx = 0.151, ke = 30, kc = 100.

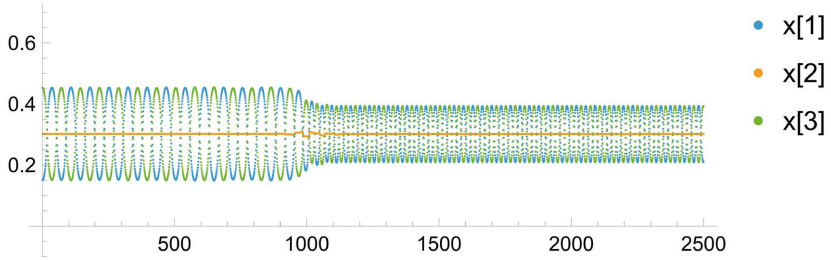

Figure 22. Neutron quark orbits x1, x2, x3 for force parameters: kx = 0.151, ke = 30, kc = 100.

The above dynamics were calculated for protons with quarks u-d-u, and various combinations of scaling parameters. This model is not a *proton* model but a *hadron* model, and therefore the model should also work to simulate neutrons, with d-u-d quarks. In Figure 22, the same scaling parameters apply to the neutron as were used for the proton in Figure 20. Interestingly, the initial oscillations of the

neutron's quark orbits appear more stable than those of the proton, however the instability appears in the neutron about time step 1000, whereas the corresponding proton instability occurred after time step 1500, as seen in Figure 21. This might be reasonable, as protons appear to last forever, whereas isolated neutrons decay with a half-life on the order of ten minutes. Comparison of Figure 21 to Figure 23 seems to indicate a lower C-field energy density is associated with the stable state of neutron than with the corresponding state of the proton.

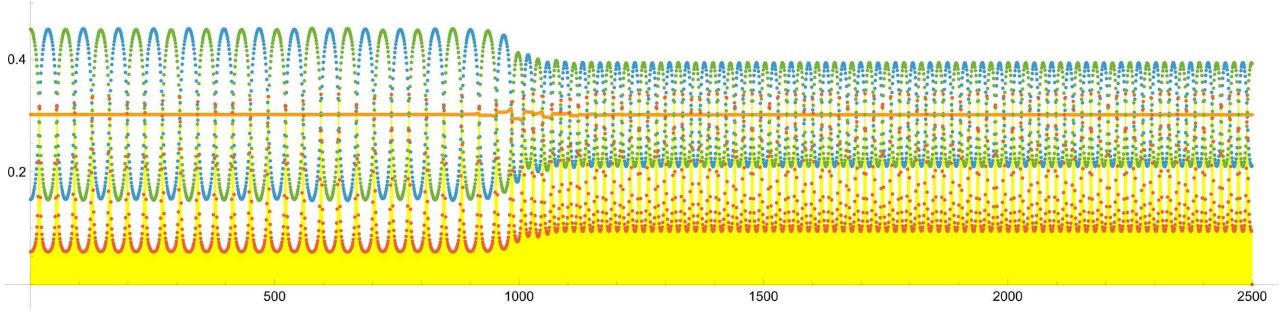

Figure 23. Energy diagram for neutron dynamics: kx = 0.151, ke = 30, kc = 100.

10. Summary and Conclusions

The QGD hadron model works for protons and neutrons, yielding different values for proton versus neutron, a desirable outcome for hadron simulation. We are far from proving that QGD explains all of the collider data upon which the Standard Model is based, but we have seen that the intuitive model derived from Primordial Field Theory explains physical phenomena associated with the strong force and string theory without invoking chromodynamic color, which was introduced to solve a perceived Pauli Principle-based problem. The mass-current-based flux tube nature of the solution bears some similarity to chromoelectric flux tubes derived from lattice-QCD simulations, but is far more intuitive, being based on the Heaviside duality of electrodynamics and gravito-dynamics, and being equivalent to General Relativity, which QCD is decidedly not.

This paper provides the first quantitative dynamical treatment of a QGD hadron model with scaling parameters for gravitodynamics forces [kf] and electrodynamic forces [ke] and orbital scaling [kr], as well as allowing initial position scaling, [kx]. The primary question to be answered is *whether the model yields stable states of hadrons*. The answer appears to be yes. That is the key result of this paper. The next question is whether the model yields known physical results. The primary unresolved physics has to do with the mass density of fermions, specifically quarks, and the central place of parameter ρ in Equation (5). Determination of this density will help nail down appropriate values of scaling parameters. The density is not measurable; hence its value must be determined by simulation results that match experimental hadron data. That is not expected to be a simple task, but the model and simulation tools presented in this paper provide a starting point for this process. If the process is successful, we hope to next quantitatively model

quark confinement. However, it is expected that it will be possible to explain other physical phenomena that cannot yet be explained by QCD, before satisfactorily determining the quark mass densities. By far the greatest proportion of QCD flux tube simulations is based on mesons, consisting of a quark-anti-quark pair. 3-quark hadron QCD flux models investigate L-shaped, T-shaped, and Y-shaped flux architectures, since what is really going on inside the hadron is unknown. However, there is a large body of theory that seems to require QCD color to obtain the fit to collider data; this fact requires more analysis. These issues provide direction for continued investigations of the QGD hadron model.

Conflicts of Interest

The author declares no conflict of interest regarding the publication of this paper.

References

[1] Cea, P., Cosmai, L., Cuteri, F. and Papa, A. (2017) Flux Tubes in the QCD Vacuum. *Physical Review D*, **95**, Article 114511. https://doi.org/10.1103/physrevd.95.114511

[2] Klingman, E.E. (2025) The Origin of the Strong Force in Quantum Gravity. *Journal of Modern Physics*, **16**, 198-227. https://doi.org/10.4236/jmp.2025.161009

[3] Klingman, E. (2024) Calabi-Yau Topology of Primordial Fermions. *Journal of Modern Physics*, **15**, 132-158.

[4] Smith, J. (2018) Rotational Energy as Mass in H_3^+. *Physical Review Letters*, **120**, Article 143002.

[5] Hestenes, D. and Sobczyk, G. (1984) Clifford Algebra to Geometric Calculus. Reidel Publication.

[6] Heaviside, O. (1893) A Gravitational and Electromagnetic Analogy. *The Electrician*, **31**, 81-88.

[7] Will, C.M. (2018) New General Relativistic Contribution to Mercury's Perihelion Advance. *Physical Review Letters*, **120**, Article 191101. https://doi.org/10.1103/physrevlett.120.191101

[8] Klingman, E.E. (2021) Encoding Energy-Density as Geometry. *Journal of Modern Physics*, **12**, 1190-1209. https://doi.org/10.4236/jmp.2021.129073

[9] Jefimenko, O. (2000) Causality, Electromagnetic Induction & Gravitation. 2nd Edition, Electret Scientific Company.

[10] Klingman, E. (2023) Ontology of Relativistic Mass. *Journal of Modern Physics*, **14**, 741-754.

[11] Klingman, E. (2024) The Origin of Electric Charge in Quantum Gravity. *Journal of Modern Physics*, **15**, 511-535.

[12] Duckworth, H. (1960) Electricity and Magnetism. Holt, Rinehart and Winston, Inc.

[13] Huang, K. (2017) A Superfluid Universe. World Scientific.